HIGH POWER, HIGH INTENSITY SUPERCONDUCING PROTON DRIVER LINAC AT KEK

Gunn Tae Park*, Eiji Kako, Yukinori Kobayashi, Tadashi Koseki, Tomofumi Maruta,
Shinichiro Michizono, Fujio Naito, Hirotaka Nakai, Kensei Umemori, and Seiya Yamaguchi
High Energy Accelerator Research Organization (KEK), Tsukuba, Japan

Abstract

At High Energy Accelerator Organization (KEK), there has been a preliminary investigation on building a linac-based multi-MW, high intensity proton driver for neutrino experiments. We report some preparations toward the front end design of the driver linac: front end beamline structure and the designs of two superconducting cavities, the half-wave resonator 1 and half-wave resonator 2.

INTRODUCTION

At the KEK, there has been a discussion on upgrading the beam power of the proton to ~ MW for frontier physics experiments with neutrinos and quarks. In particular, many important discoveries on long-baseline neutrino oscillation can be made with high intensity proton beam [1]. The main limitation on power upgrade in circular accelerator, space charge effect leading to beam instabilities, can be more easily overcome with the linear accelerator. The KEK is considering to build a new high intensity, high power proton driver linac that provides 9 MW proton beam at 9 GeV with average beam current of 1 mA. The proton is accelerated in pulsed operation at the peak current 100 mA with duty factor of 1%. The beam parameters are summarized in Table 1.

Table 1: Beam Parameters of the Driver

Beam parameters	Unit	Value
Beam energy	GeV	9
Beam (peak) current	mA	100
Beam power	MW	9
Pulse length	ms	1
Repetition rate	Hz	10

The accelerator will be located at KEKB tunnel of the KEK, whose schematic view is given in Fig. 1. In KEKB tunnel, there are 4 straight sections which can host linac structure. While the proton beam will be accelerated by 9-cell ILC cavities in the 2nd, 3rd, and 4-th section, the 1st section called front-end consists of low-beta accelerators from the source to 1.2 GeV.

In particular, a high intensity beam poses challenges on many fronts of the accelerator technology. For example, hands-on maintenance without significant residual radiation is available when the power deposit per length due to beam loss does not exceed 1 W/m. More careful focusing to avoid halo formation along the beamline is needed for low beam
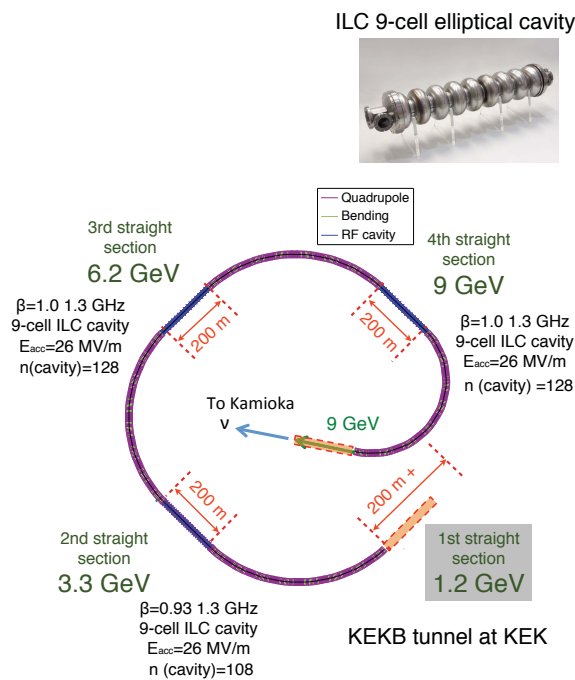
* gunnpark@post.kek.jp

Figure 1: The tunnel configuration of the proton driver.

loss rate control. To sustain a high beam power, MW-power coupler needs to be developed and heavy beam loading must be controlled by extreme over-coupling.
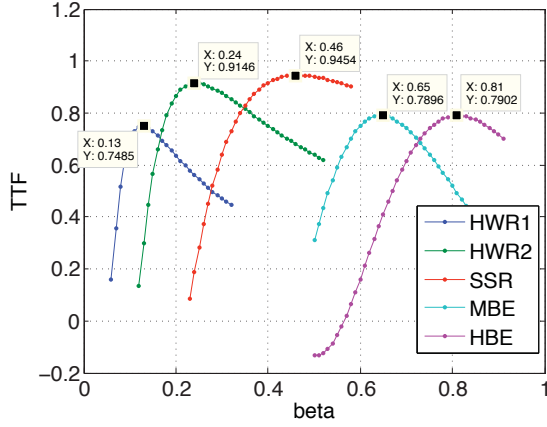
FRONT END OF THE LINAC

The front-end, whose schematic structure is given in Fig. 2(a), accelerates the proton beam from ion source to 1.2 GeV. The continuous beam from the ECR (Electron cyclotron resonator) ion source, after shrink by solenoid in low energy beam transport (LEBT) and is focused, bunched, and accelerated by the RFQ (radiofrequency quadrupole) at very low energy. After the RFQ, the beam is collimated and bunched more by a series of bunchers in medium energy beam transport (MEBT) before it goes through the accelerators. The accelerators in front-end are 5 different kinds of superconducting cavities: 3 low-beta superconducting cavities-half-wave resonator 1 (HWR1), half-wave resonator 2 (HWR2), and single spoke resonator (SSR)-and 2 reduced elliptical cavities-medium beta elliptical cavity (MBE) and high beta elliptical cavity (HBE). The transit time factor structure and energy gain of the proton is shown in Fig. 2(b).

For a low beam loss rate, specially in low energy region, tighter focusing period is needed and superconducting
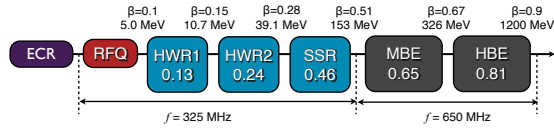
(a) The front end structure of the linac

(b) The transit time structure.

Figure 2: The front-end design of the driver linac.

Table 2: RF Parameters of Linac Components

Parameters	HWR1	HWR2	SSR	MBE	HBE
f (MHz)	325	325	325	650	650
$n_{cell/gap}$	2	2	2	5	5
β_{opt}	0.13	0.24	0.46	0.61	0.76
β_{in}	0.1	0.15	0.28	0.51	0.67
β_{out}	0.15	0.28	0.51	0.67	0.9
V_0 (MV)	0.7	2.1	5.3	10.2	15.4
ϕ_s (°)	−30	−30	−27	−27	−27
G (Ω)	40	73	117	192	236
E_{sp}/E_{acc}	6.9	4.8	4.1	2.5	2.4
B_{sp}/E_{acc}	14.2	6.2	7.9	4.6	4.4
P_{beam} (kW)	53	182	473	909	1373
n_{cav}	10	20	30	20	72
$n_{cryomodule}$	2	5	6	5	24

The unit for B_{sp}/E_{acc} is mT/(MV/m).

solenoids will be inserted after almost every superconducting cavity within the cryomodule. The specifications of each component in the front-end is listed in Table 2.

ELECTROMAGNETIC DESIGN OF THE TWO CAVITIES

The first two superconducting cavities in the front-end are half-wave resonator 1 (HWR1) and half-wave resonator 2 (HWR2), low-β cavities based on coaxial-structure with TEM-like modes.

Important features of the cavities

Two half-wave resonators (HWR's) have the following features (See Fig. 3).
For low beam loss control, the apertures of the beam ports were maximized for both cavities. Assuming Gaussian beam profile, the *rms* beam sizes were $\sigma_1 = 3.1$ mm for the HWR1 and $\sigma_2 = 2.2$ mm for the HWR2, respectively. Imposing roughly around 10^{-5} loss rate (equivalent to 1 W/m) with margin for alignment errors, the apertures were set to be $\phi_1 = \phi_2 = 40$ mm. The re-enetrant nose was introduced to maintain the gap structure as the outer housing radius is increased, which improves the many figures of merit. Tapering of the center conductors was introduced to minimize the peak magnetic field B_{sp} by flattening the field distribution over the stem. In case of the HWR1, with requirement for the tightest beam focusing as the first accelerating structure in front-end, axis-symmetric accelerating field is most required, because the superconducting solenoid has only axis-symmetric focusing field. Thus the HWR1 has donut shaped drift tube, which is known to have axis-symmetric accelerating field [2]. In HWR2, race-track drift tube was introduced instead for higher accelerating voltage. In addition, the near the base of the tapered center conductors, the cylindrical parts were added for straightforward machining during the pre-tuning.
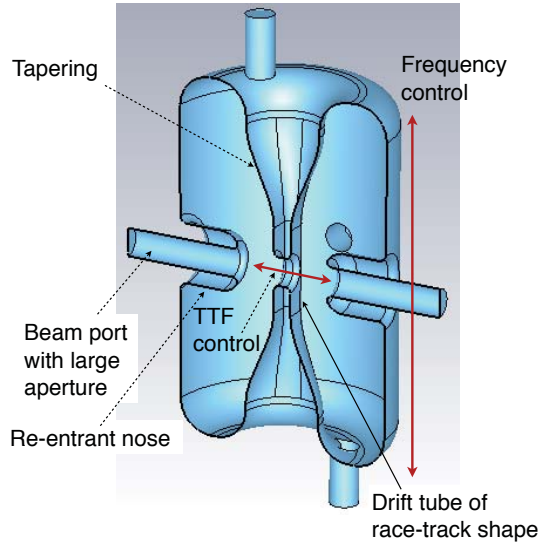
Optimization

The optimization is done for a set of figures of merit, the ratio of electric surface peak field to accelerating gradient E_{sp}/E_{acc}, the ratio of magnetic surface peak field to accelerating gradient B_p/E_{acc}, the geometrical factor G, and two constraints on f and β_{opt} as given in Table 2. Using 3D FEA (finite element analysis) code CST-MWS [3], the geometrical parameters of the cavities were swept while tracking the figures of merit. First we establish the mesh number for accurate evaluation of E_{sp}, which determines the scaling factor to target values of all the other figures of merit. The target values are at $E_{sp} = 35$ MV/m.

In Fig. 4, we found the 3.6 million and 4.1 million meshes are needed for HWR1 and HWR2, respectively. In addition, a number of fixed points that generates finer local meshes were fed into the model as geometry becomes more complicated.

In the sweep (which is consistent with the procedures in [4]), the frequencies of the cavities were mainly controlled by H, while the TTF's were mainly by d and g. The control of TTF is technically more challenging because, B_{bore}, B_{nose}, B_{tube} also affect the TTF and the range of control by d and g is limited and might deteriorate the accelerating
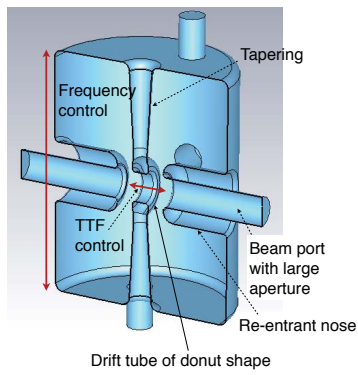
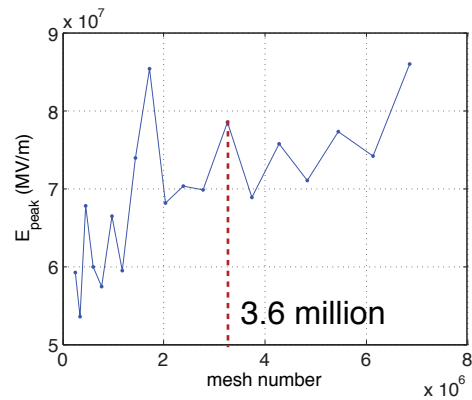(a) The features of the HWR1.

(b) The features of the HWR2.

Figure 3: The important features of the two cavities.

(a) HWR1

(b) HWR2

Figure 4: The E_p vs. mesh numbers.

$T = 4$ K, expected operation temperatures of the two cavities.

Table 3: Figures of Merit

Figures of merit	HWR1	HWR2
V_0 (MV)	0.86	1.93
TTF	0.77	0.79
V_{acc} (MV)	0.66	1.52
E_{acc} (MV/m)	5.5	6.9
Q_0	1.1×10^9	1.9×10^9
G (Ω)	53.8	88.3
R/Q_0 (Ω)	237.7	120.8
E_{sp}/E_{acc}	6.3	5.1
B_{sp}/E_{acc} (mT/(MV/m))	12.9	8.3
U (J)	0.9	4.4
P_{wall} (W)	1.6	4.8

gradient. In the HWR1, 14 parameters were swept for the optimization and some of the sweep results are shown in Fig. 5. The increasing gap size g has tendency to increase V_{acc}. Tapering was optimized in terms of ratio R_{top}/R_{bottom} to minimize the peak magnetic field.

In HWR2, 14 parameters were swept for the optimization. Some of the sweep results are shown in Fig. 6. The geometry of race-track was optimized to maximize the E_{sp}/E_{acc}. As in the HWR1 case, the blending radii in gap structure tend to increase the accelerating voltage.

RF performance of the cavities

The RF performance of the cavities, characterized by figures of merit, after optimization is listed in Table 3. In Table 3, V_0 is DC voltage across the cavity, E_{acc} is the accelerating field and defined as $E_{acc} = V_{acc}/\beta_{opt}\lambda$ where λ is wavelength of the RF field, Q_0 is (unloaded) quality factor, U is stored energy, R/Q_0 is shunt resistance over Q_0, P_{wall} is wall loss. The Q_0 value was computed based on the surface resistance $R_s = 47.4$ nΩ of high-purity niobium at

The electromagnetic fields in the cavities are shown in Fig. 7 and Fig. 8. The strong electric fields are located near beam axes, accelerating the beams. The magnetic fields are more or less uniformly distributed over the center conductors while there is little field near beam axis, without disturbing the beam.
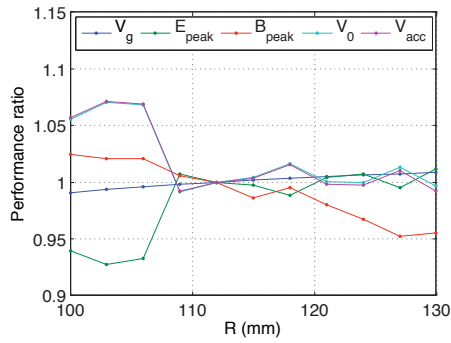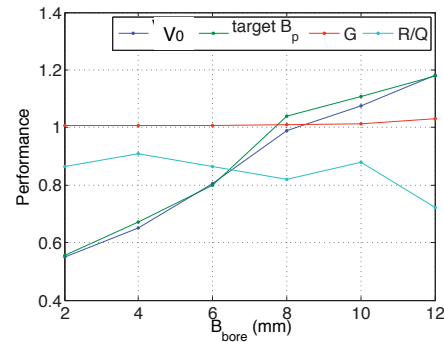
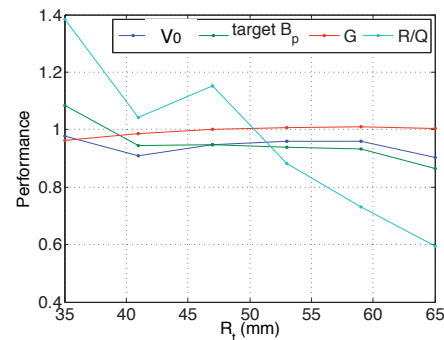(a) The radius of the outer conductor sweep.
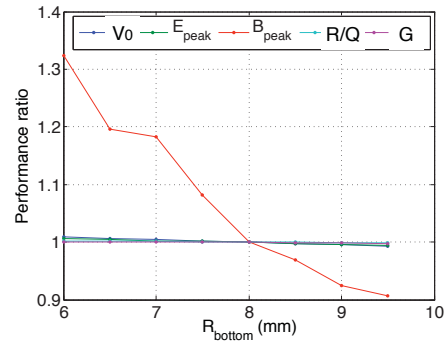
(b) The bottom radius of the center conductor sweep.
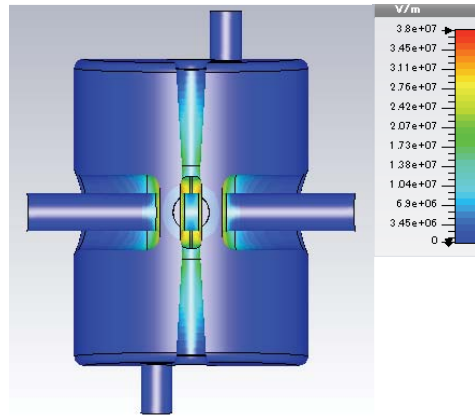
Figure 5: Some parameter sweeps of the HWR1.

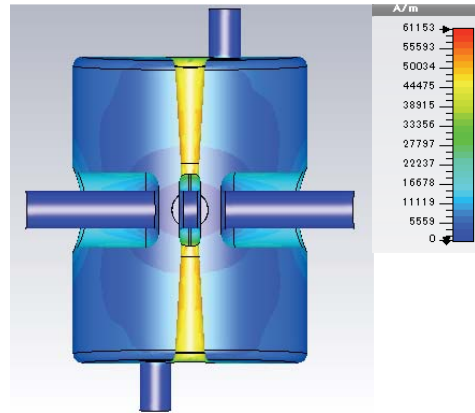(a) The blending radius of bore radius sweep.

(b) The top radius of the center conductor sweep.

Figure 6: More parameter sweeps of the HWR2.
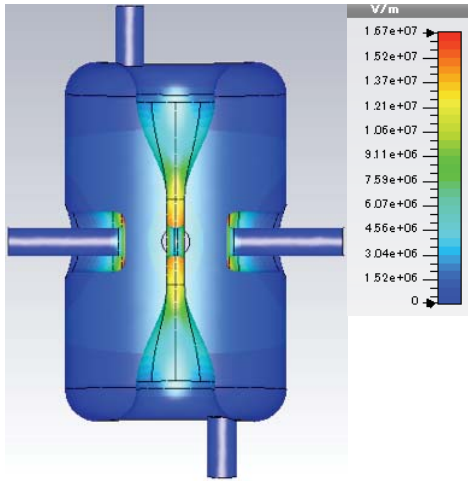

(a) The electric field of the HWR1.

(b) The magnetic field of the HWR1.

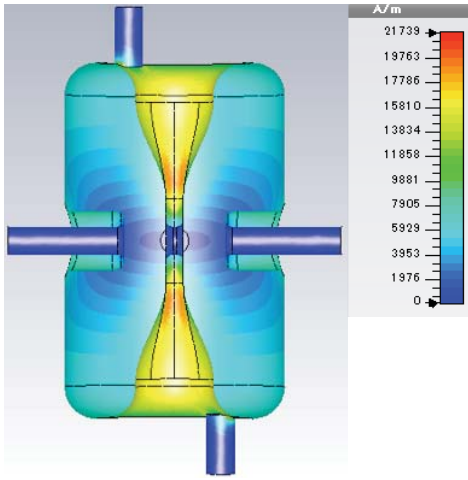Figure 7: The electromagnetic fields of the HWR1.

In case of HWR1, donut shaped drift tube minimizes the axial field asymmetry. In Fig. 9(b), the transverse field asymmetry, defined as $E_y(y = \sigma) - E_z(z = \sigma)$ with the expected *rms* beam size σ being 3.5 mm, is plotted. The maximum asymmetry is only 4×10^4 V/m, less than 1% of the accelerating field gradient. Notice that due to symmetric distribution of field asymmetry with respect to y-axis, as a particle beam passes through the y-axis, the field changing in time flips its sign, leading to smaller contribution to asymmetric deformation of the beam profile. A similar analysis was done to HWR2 in Fig. 9(c). The HWR2 has bigger field asymmetry amounting to about 1.6 % of the accelerating field. The discrepancy between two peaks in Fig. 9(c) is most likely due to irregularities in mesh.

POWER SUPPLY

With the heavy beam loading, the power is kept minimum with strong over-cpoupling ($Q_L \approx Q_e \ll Q_0$). The power supply from generator P_g to keep a constant accelerating

(a) The electric field of the HWR2.

(b) The magnetic field of the HWR2.

Figure 8: The electromagnetic fields of the HWR2.

voltage in a strong over-coupling is given by [5]

$$
P_g = \frac{V_{acc}^2}{4\frac{R}{Q_0}Q_L}\left(1 + Q_L\frac{R}{Q_0}\frac{I_b}{V_{acc}}\cos\phi_s\right)^2
$$

$$
+ \left(2Q_L\frac{\delta f}{f} - Q_L\frac{R}{Q_0}\frac{I_b}{V_{acc}}\sin\phi_s\right)^2, \qquad (1)
$$

where I_b is beam current, ϕ_s is synchronous phase, δf is arbitrary frequency deviation, and Q_L is loaded quality factor. The power in (1) increases quadratically with I_b and it is important to control the power minimum with a high beam current of $I_b = 100$ mA. The generator power as a function of δf and Q_e for the two cavities are shown in Fig. 10.

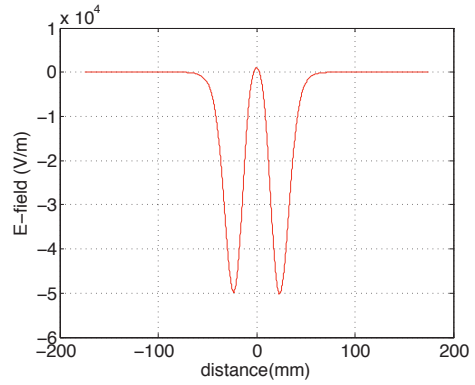From the equivalent lumped circuit point of view, the matching condition with no reflecting signals is

$$
\delta f = \frac{1}{2}\frac{R}{Q_0}\frac{I_b}{V_{acc}}f\sin\phi_s, \qquad (2)
$$

and

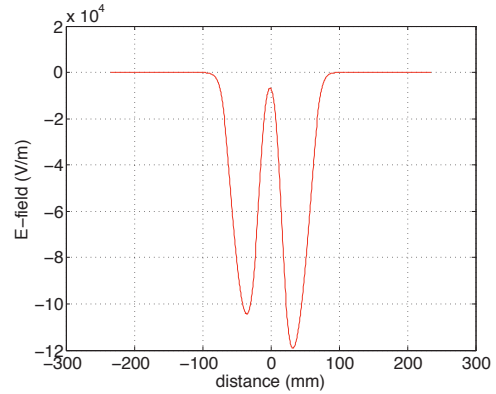$$
Q_e \approx Q_L = \frac{V_{acc}}{RI_b\cos\phi_s}Q_0. \qquad (3)
$$
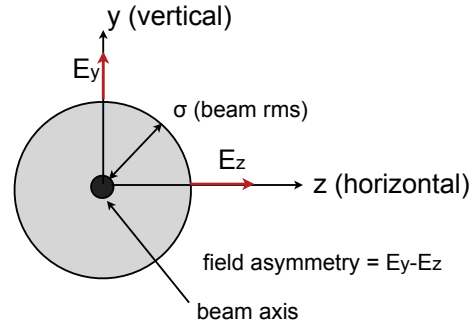
(a) The configuration of the field asymmetry.

(b) The field asymmetry of the HWR1.
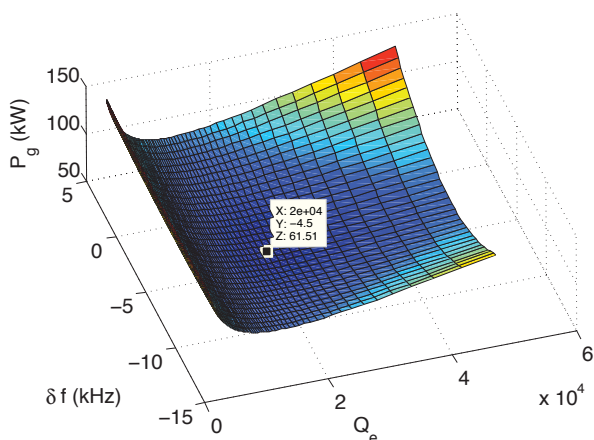

(c) The field asymmetry of the HWR2.

Figure 9: The field asymmetry of the two cavities.

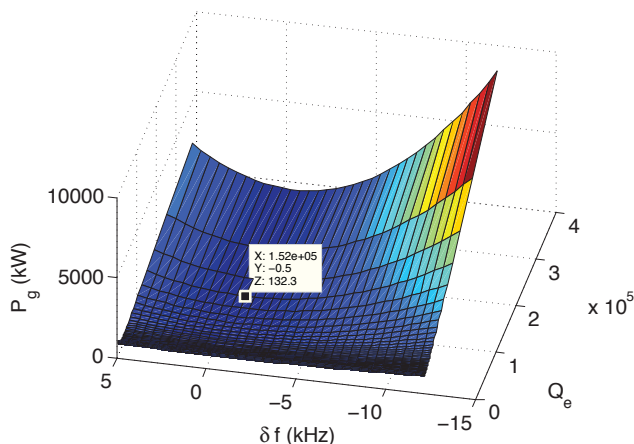These two conditions would make (1) minimum. The corresponding bandwidth $\Delta_{\pm 3dB}$ is given as

$$
\Delta_{\pm 3dB} = \frac{f}{Q_L} = \frac{R}{Q_0}\frac{I_b}{V_{acc}}f\cos\phi_s. \qquad (4)
$$

The calculated numerical values of (2), (3), (4) together with bean loading parameters for the HWR1 and the HWR2 are listed in Table 4.

(a) The power supply of the HWR1.

(b) The power supply of the HWR2.

Figure 10: The power supply with varying frequency and the coupling.

Table 4: Beam Loading Parameters

Figures of merit	HWR1	HWR2
I_b (mA)	100	100
ϕ_s (°)	-30	-30
Q_e	2.1×10^4	1.45×10^5
f_{detune} (kHz)	-4.5	-0.65
$\Delta_{\pm 3dB}$	15.7	2.37
P_g (kW)	62	132

CONCLUSION

The front-end linac design is done for the new multi-MW proton driver for long-baseline neutrino physics experiment with the decisions on specification of each component. The front-end will include 5 different superconducting cavities for the low-intermediate energy acceleration. Among them the first 2 superconducting cavities were designed satisfying the target specification.Their prototype fabrications are im-

pending. We will further report on multipacting simulation and possible design modification later.

REFERENCES

[1] U. Al-Binni *et al.*, *Project X, Physics Opportunities*, arXiv:1306.5009v2 (2013).

[2] B. Mustapha, P. N. Ostroumov, and Z. A. Conway, "Ring-shaped center conductor geometry for a half-wave resonator", *Proceedings of IPAC2012, New Orleans, LA, U.S.A.* (2012).

[3] CST simulation packages; http://www.cst.com

[4] Lixin Ge *et al.*, "Electro-magnetic optimization of a half-wave resonator", *Proceedings of SRF2011, Chicago, IL, U.S.A.* (2011).

[5] A. Neumann, W. Anders, O. Kugeler, and J. Knobloch, Phys. Rev. ST Accel. Beams **3**, 092001 (2000).